

Spin-wave and electromagnon dispersions in multiferroic MnWO_4 as observed by neutron spectroscopy: Isotropic Heisenberg exchange versus anisotropic Dzyaloshinskii-Moriya interaction

Y. Xiao (肖荫果),^{1,*} C. M. N. Kumar,^{2,3,†} S. Nandi,^{1,4,5} Y. Su (苏夷希),⁴ W. T. Jin (金文涛),^{1,4} Z. Fu (付振东),⁴ E. Faulhaber,^{6,7} A. Schneidewind,^{4,7} and Th. Brückel^{1,4}

¹Jülich Centre for Neutron Science and Peter Grünberg Institut, JARA-FIT, Forschungszentrum Jülich GmbH, 52425 Jülich, Germany

²Jülich Centre for Neutron Science, Forschungszentrum Jülich GmbH, Outstation at SNS, POB 2008, 1 Bethel Valley Road, Oak Ridge, Tennessee 37831-6473, USA

³Chemical and Engineering Materials Division, Oak Ridge National Laboratory, Oak Ridge, Tennessee 37831, USA

⁴Jülich Centre for Neutron Science at Heinz Maier-Leibnitz Zentrum, Forschungszentrum Jülich GmbH, Lichtenbergstraße 1, 85747 Garching, Germany

⁵Department of Physics, Indian Institute of Technology, Kanpur 208016, India

⁶Heinz Maier-Leibnitz Zentrum, Technische Universität München, Lichtenbergstraße 1, 85748 Garching, Germany

⁷Helmholtz-Zentrum Berlin für Materialien und Energie, Hahn-Meitner-Platz 1, D-14109 Berlin, Germany

(Received 19 January 2016; revised manuscript received 18 April 2016; published 21 June 2016)

High-resolution inelastic neutron scattering reveals that the elementary magnetic excitations in multiferroic MnWO_4 consist of low-energy dispersive electromagnons in addition to the well-known spin-wave excitations. The latter can well be modeled by a Heisenberg Hamiltonian with magnetic exchange coupling extending to the 12th nearest neighbor. They exhibit a spin-wave gap of 0.61(1) meV. Two electromagnon branches appear at lower energies of 0.07(1) and 0.45(1) meV at the zone center. They reflect the dynamic magnetoelectric coupling and persist in both the collinear magnetic and paraelectric AF1 phase and the spin spiral ferroelectric AF2 phase. These excitations are associated with the Dzyaloshinskii-Moriya exchange interaction, which is significant due to the rather large spin-orbit coupling.

DOI: [10.1103/PhysRevB.93.214428](https://doi.org/10.1103/PhysRevB.93.214428)

I. INTRODUCTION

Multiferroics with strong coupling between ferroelectric and ferromagnetic degrees of freedom have attracted intense research effort due to their application potential in tunable multifunctional devices [1–5]. So-called spin-driven ferroelectrics, for which the inversion symmetry is broken in the ferroelectric phase due to the appearance of a particular magnetically ordered state, provide a path to the required coupling [6,7]. It was found that spin-driven ferroelectricity can occur in different magnetic materials with different types of magnetic ordering states. In order to understand magnetoelectric (ME) coupling in spin-driven ferroelectrics, three different microscopic models, namely, the exchange striction model, inverse Dzyaloshinskii-Moriya (DM) model, and spin-dependent p - d hybridization model, have been proposed to describe the observed ferroelectricity in different spin-driven ferroelectrics [8–10].

The inequivalent exchange striction induced by the symmetry spin-exchange interaction between the neighboring spins is considered as the driving force of ferroelectricity for multiferroics with commensurate spin order and low symmetry on the specific chemical lattice, such as $\text{Ca}_3(\text{Co},\text{Mn})\text{O}_6$ [11] and RMn_2O_5 ($R = \text{Tb-Lu}$) [12]. The inverse DM model arising from the antisymmetric spin-exchange interaction between canted spin sites can be used to describe the emergence of ferroelectricity for multiferroics with transverse screw spin

configurations, such as RMnO_3 ($R = \text{Gd, Tb, Dy}$) [13] and $\text{Ni}_3\text{V}_2\text{O}_8$ [14] with cycloidal spin order and CoCr_2O_4 [15] and $(\text{Sr},\text{Ba})_3\text{Co}_2\text{Fe}_{24}\text{O}_{41}$ with transverse-conical spin order [16]. According to the inverse DM model, electric polarization is produced through the spin-orbit interaction by displacing anions between two canted magnetic moments. It is worthwhile to note that multiferroicity around room temperature has been discovered in conical hexaferrite systems [16,17], although the ME effect in them is still too small for practical application. Unlike the exchange striction model and inverse DM model, the spin-dependent p - d hybridization model predicts the appearance of electric polarization along a certain bond direction due to the spin-direction dependent hybridization arising from the spin-orbit coupling. A typical multiferroic system based on the spin-dependent p - d hybridization is CuFeO_2 with proper screw spin order [18].

Given that strong coupling between the magnetic and ferroelectric orders exists intrinsically in spin-driven ferroelectrics, magnetic field control of spontaneous polarization and/or electric-field control of the magnetization have been successfully demonstrated in several spin-driven multiferroics [15,19]. Moreover, the cross-control between electric and magnetic dipoles in multiferroics is found to be accompanied by the dynamical motion of multiferroic domain walls [19–21]. In addition, the dynamic magnetoelectric coupling in multiferroics will lead to the appearance of electric-dipole-active magnetic resonance, i.e., a novel collective excitation named the electromagnon [22]. The identification of an electromagnon by terahertz spectroscopy and neutron scattering confirmed the existence of this dynamical magnetoelectric coupling [22–27].

*y.xiao@fz-juelich.de

†n.kumar@fz-juelich.de

As a prototypical multiferroic material with spiral magnetic order, MnWO_4 has been widely studied concerning its magnetic and ferroelectric properties [28–38]. It is well accepted that the inverse DM mechanism is relevant for modeling the ME coupling in MnWO_4 . Similar to the case of multiferroic TbMnO_3 , the magnetically induced electric polarization in MnWO_4 fulfills the relation

$$\vec{P} = A \vec{e}_{ij} \times (\vec{S}_i \times \vec{S}_j). \quad (1)$$

Here A is a coupling coefficient and \vec{e}_{ij} is the unit vector connecting two neighboring Mn moments \vec{S}_i and \vec{S}_j . However, it is argued that DM interaction is not the only driving force for the ferroelectric polarization; other single-site symmetric interactions are also shown to be involved in the magnetoelectric process in MnWO_4 [39]. Besides, a theoretical study suggests a more complex scenario where multiferroicity in MnWO_4 is caused by a competition of DM and isotropic exchange interactions [40]. A deeper insight into the coupling between the electric and magnetic degrees of freedom can be gained by studying not only the respective order but also the excitation spectra.

In this paper, we report the observation of elementary magnetic excitations in multiferroic MnWO_4 by high-resolution inelastic neutron scattering. A detailed analysis of the low-energy excitations of MnWO_4 shows that the spin-wave excitations in the collinear antiferromagnetic/paraelectric phase can be well described by a Heisenberg model with magnetic exchange couplings extending to the 12th nearest neighbor, although MnWO_4 was considered as a moderately spin frustrated system. In addition, the electromagnon excitation observed in both the paraelectric and ferroelectric phases supports the existence of strong spin-orbit interaction in MnWO_4 , despite the fact that Mn^{2+} is an S -state ion.

II. EXPERIMENT

Single crystals of MnWO_4 were grown by floating-zone method. The heat-capacity measurement was performed by using a quantum design physical property measurement system. Single-crystal neutron diffraction and inelastic neutron spectroscopy were performed on the cold-neutron triple-axis spectrometer PANDA operated by Jülich Centre for Neutron Science at the Maier-Leibnitz Zentrum in Garching, Germany [41]. The crystal used for the neutron-scattering measurements has the shape of a cylinder with a total mass of 5.1 g. For the inelastic neutron-scattering measurements, pyrolytic graphite PG(002) were selected as monochromator and analyzer, while a Be filter was placed before the analyzer. The final neutron wave vector was fixed to $k_f = 1.2 \text{ \AA}^{-1}$. In what follows we will describe the neutron-scattering data in the high-symmetry monoclinic $P2/c$ space group with scattering vector $\mathbf{Q} = (q_x, q_y, q_z)$ (in units of \AA^{-1}) at position $(HKL) = (q_x a/2\pi, q_y b/2\pi, q_z c/2\pi)$ in reciprocal-lattice units, where $a = 4.8226(3) \text{ \AA}$, $b = 5.7533(6) \text{ \AA}$, $c = 4.9923(5) \text{ \AA}$, and $\beta = 91.075(7)^\circ$ at $T = 1.5 \text{ K}$ [42]. The MnWO_4 single crystal was aligned in the scattering plane defined by the orthogonal vectors $(1\ 0\ 2)$ and $(0\ 1\ 0)$, in which low-energy excitations along main symmetry directions in the magnetic Brillouin zone can be surveyed.

III. EXPERIMENTAL RESULTS AND MODELING

A. Antiferromagnetic order in MnWO_4

MnWO_4 crystallizes in monoclinic $P2/c$ structure. It consists of MnO_6 octahedra with Mn^{2+} (d^5) ions as well as W^{6+} (d^0) ions [43]. The high-spin Mn^{2+} ion with the d -orbital configuration $t_{2g}^3 e_g^2$ is the only magnetic ion in the MnWO_4 unit cell. Below the magnetic ordering temperature ($T_N = 13.5 \text{ K}$), MnWO_4 undergoes three successive magnetic transitions. The corresponding phases are labeled as AF1, AF2, and AF3 [42]. The AF1 phase below 7.8 K is a commensurate antiferromagnetic phase with wave vector $\mathbf{k}_C = (\pm 1/4, 1/2, 1/2)$ as illustrated in Fig. 1(a). Between 7.8 and 12.6 K, the AF2 phase with incommensurate (IC) spiral spin structure prevails. An incommensurate propagation vector $\mathbf{k}_{IC} = (-0.214, 1/2, 0.457)$ has been reported for the AF2 phases. With further increase in temperature the AF3 phase appears, with the Mn^{2+} moment order in an incommensurate collinear antiferromagnetic configuration with the same magnetic wave vector as in the AF2 phase [42].

As shown in Fig. 1(b), the magnetic phase transitions in MnWO_4 are visible in both Q scans through the magnetic $(1/4, 1/2, 1/2)$ reflection and specific-heat curve. The lock-in transition between AF2 and AF1 takes place at 7.8 K.

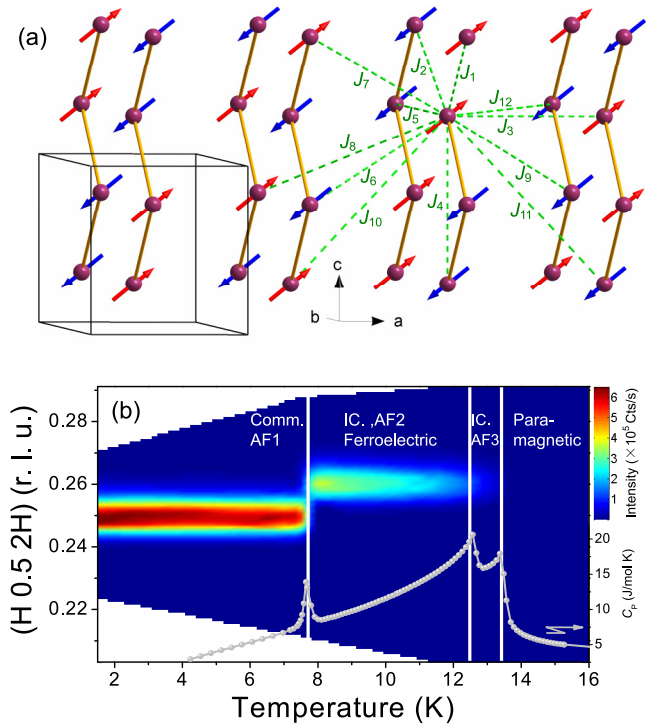


FIG. 1. (a) Schematic drawing of the crystal and magnetic structure of the AF1 phase of MnWO_4 showing the magnetic Mn^{2+} ions only. Solid lines highlight the monoclinic unit cell. The arrows on the Mn atoms denote the directions of their spins and the dashed lines denote the paths of Heisenberg exchange interactions. (b) Evolution of magnetic modulation $(1/4, 1/2, 1/2)$ with increasing temperature. The dots denote the temperature dependence of the molar specific-heat measurement. Four distinct phases labeled as AF1, AF2, AF3, and paramagnetic are revealed. Comm. and IC. denote commensurate and incommensurate modulation, respectively.

Subsequently, an incommensurate wave vector is observed around (0.26(1), 1/2, 0.52(1)) for the AF2 and AF3 phases. It should be noted that the observed wave vector located at (0.26(1), 1/2, 0.52(1)) in the AF2 phase is equivalent to the $\mathbf{k}_{\text{IC}} = (-0.214, 1/2, 0.457)$ reported in [42]. Indeed, the signal at (0.26(1), 1/2, 0.52(1)) comes from the adjacent IC magnetic reflection (0.214, 1/2, 0.543), which can be indexed by $(0\ 1\ 1)_N\text{-}\mathbf{k}_{\text{IC}}$.

B. Spin-wave dispersion and analysis

The observed low-energy excitations in the AF1 phase at 1.5 K along the [1 0 2] and [0 1 0] directions through the magnetic peak (1/4, 1/2, 1/2) are shown in Figs. 2(a) and 2(c), respectively. Because MnWO₄ is an antiferromagnetic insulator with a rather large ordered Mn moment, we analyze inelastic neutron-scattering data in the linear spin-wave approximation with a Heisenberg Hamiltonian [44]:

$$H = -\frac{1}{2} \sum_{i,j} J_{ij} \mathbf{S}_i \cdot \mathbf{S}_j - D_s \sum_i \mathbf{S}_{i,z}^2. \quad (2)$$

Here J_{ij} denote exchange constants (from J_1 to J_{12}), while D_s is the uniaxial single-ion anisotropy constant.

In the collinear AF1 phase, the magnetic unit cell of MnWO₄ contains in total eight spins, i.e., four up spins (labeled as i with $i = 1, 2, 3, 4$) and four down spins (labeled as j with $j = 1, 2, 3, 4$). The linearized Holstein-Primakoff transformation for the quantum spin \hat{S} at each site is given as

$$\hat{S}_i^\dagger = \sqrt{2S} \left(1 - \frac{a_i^\dagger a_i}{2S} \right)^{1/2} a_i \approx \sqrt{2S} a_i, \quad (3a)$$

$$\hat{S}_i^- = \sqrt{2S} \left(1 - \frac{a_i^\dagger a_i}{2S} \right)^{1/2} a_i^\dagger \approx \sqrt{2S} a_i^\dagger, \quad (3b)$$

$$\hat{S}_i^z = S - a_i^\dagger a_i, \quad (3c)$$

$$\hat{S}_j^\dagger = \sqrt{2S} \left(1 - \frac{b_j^\dagger b_j}{2S} \right)^{1/2} b_j^\dagger \approx \sqrt{2S} b_j^\dagger, \quad (4a)$$

$$\hat{S}_j^- = \sqrt{2S} \left(1 - \frac{b_j^\dagger b_j}{2S} \right)^{1/2} b_j \approx \sqrt{2S} b_j, \quad (4b)$$

$$\hat{S}_j^z = -S + b_j^\dagger b_j. \quad (4c)$$

The Fourier transformation for bosonic operators is

$$\hat{a}_i^\dagger = \sqrt{\frac{1}{N}} \sum_q e^{-iq \cdot r_i} a_q^\dagger, \quad (5a)$$

$$\hat{b}_j^\dagger = \sqrt{\frac{1}{N}} \sum_q e^{-iq \cdot r_j} b_q^\dagger, \quad (5b)$$

$$\hat{a}_i = \sqrt{\frac{1}{N}} \sum_q e^{iq \cdot r_i} a_q, \quad (5c)$$

$$\hat{b}_j = \sqrt{\frac{1}{N}} \sum_q e^{iq \cdot r_j} b_q. \quad (5d)$$

By using Holstein-Primakoff transformation, we can obtain the bosonic Hamiltonian in the momentum space as

$$H = -\frac{1}{2} \sum_q \psi_q^\dagger \mathcal{H}_q \psi_q \quad (6)$$

where $\psi_q^\dagger = (a_{q1}^\dagger a_{q2}^\dagger a_{q3}^\dagger a_{q4}^\dagger b_{-q-1}^\dagger b_{-q-2}^\dagger b_{-q-3}^\dagger b_{-q-4}^\dagger)$,

$$\mathcal{H}_q = S \begin{pmatrix} H_0 & A & B & C & E & F & -B & C^* \\ A^* & H_0 & C & D & F^* & E & C^* & -D \\ B^* & C^* & H_0 & A^* & -B^* & C & E & F^* \\ C^* & D^* & A & H_0 & C & -D^* & F & E \\ E & F & -B & C^* & H_0 & A & B & C \\ F^* & E & C^* & -D & A^* & H_0 & C & D \\ -B^* & C & E & F^* & B^* & C^* & H_0 & A^* \\ C & -D^* & F & E & C^* & D^* & A & H_0 \end{pmatrix}$$

with

$$\begin{aligned} H_0 &= 2(J_4 + J_5 + J_6 - J_7 - J_8 + J_9 - D_s), \\ A &= J_7 e^{iq_x + (2y-1)iq_y - 0.5iq_z} + J_7 e^{-iq_x + (2y-1)iq_y + 0.5iq_z} + J_8 e^{-iq_x + (2y-2)iq_y - 0.5iq_z} + J_8 e^{iq_x + (2y-2)iq_y + 0.5iq_z}, \\ B &= J_1 e^{(2y-1)iq_y + 0.5iq_z} + J_2 e^{(2y-2)iq_y - 0.5iq_z}, \\ C &= J_3 e^{iq_x} + J_{10} e^{-iq_x - iq_z} + J_{11} e^{-iq_x + iq_z} + J_{12} e^{-iq_x - iq_y} + J_{12} e^{-iq_x + iq_y}, \\ D &= J_1 e^{(1-2y)iq_y + 0.5iq_z} + J_2 e^{(2-2y)iq_y - 0.5iq_z}, \\ E &= 2J_4 \cos(q_z) + 2J_5 \cos(-q_y), \\ F &= J_6 e^{-iq_x + (2y-1)iq_y - 0.5iq_z} + J_6 e^{iq_x + (2y-1)iq_y + 0.5iq_z} + J_9 e^{iq_x + (2y-2)iq_y - 0.5iq_z} + J_9 e^{-iq_x + (2y-2)iq_y + 0.5iq_z}. \end{aligned}$$

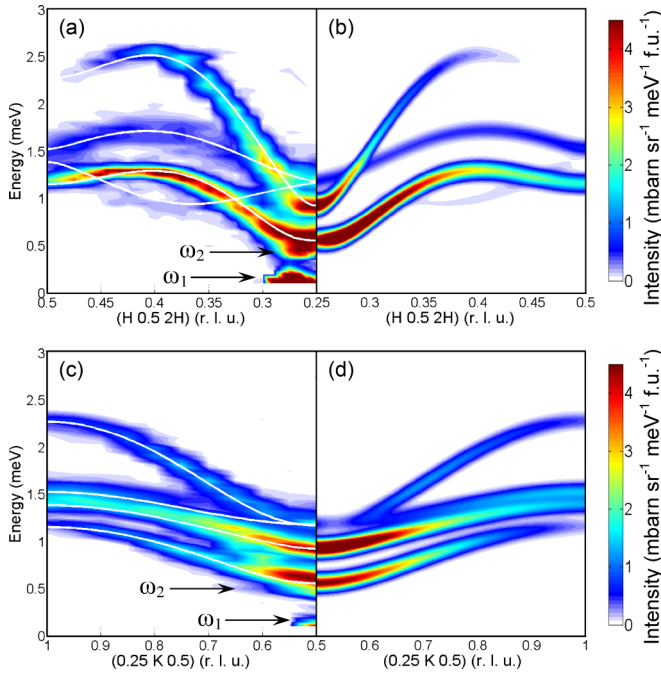


FIG. 2. The measured spin-wave spectrum compared to calculations based on a Heisenberg model that describes the antiferromagnetic ground state of MnWO_4 . (a) and (c) Experimental low-energy excitations along $[1\ 0\ 2]$ and $[0\ 1\ 0]$ directions at temperature of 1.5 K. The spectrum is composed of 16 constant- Q scans at various wave vectors. The solid lines demonstrated the spin-wave dispersion relationship resulting from a fit of the dispersion relations employing a Heisenberg Hamiltonian as described in the text. (b) and (d) Calculated spin-wave excitations of MnWO_4 in comparison with measured ones. The color code represents the intensity of inelastic scattered neutrons.

In order to obtain the eigenvalues and eigenvectors for the spin-wave modes, the bosonic Hamiltonian is diagonalized numerically. To interpret the inelastic neutron-scattering data, we connect the experimental results with theoretical calculation by using the inelastic neutron-scattering cross section. The inelastic neutron-scattering cross section can be written as

$$\frac{d^2\sigma}{d\Omega dE} = \frac{k_f}{k_i} \left(\frac{1}{2} \gamma r_0 g F(\mathbf{Q}) \right)^2 e^{-2W} \times \sum_{\alpha, \beta} (\delta_{\alpha, \beta} - \hat{Q}_\alpha \hat{Q}_\beta) S^{\alpha\beta}(\mathbf{Q}, \omega). \quad (8)$$

Here k_f and k_i are final and incident wave vectors, respectively. $\gamma r_0 = 5.39 \text{ fm}$ is the magnetic scattering amplitude for an electron. g is the Landé g factor of Mn, $F(\mathbf{Q})$ is the form factor for magnetic ion Mn^{2+} , and e^{-2W} is the Debye-Waller factor. \hat{Q}_α is the component of a unit vector in the direction of \mathbf{Q} , and $S^{\alpha\beta}(\mathbf{Q}, \omega)$ is the response function describing spin correlations [45]. Only the transverse correlations contribute to the linear spin-wave cross section through single magnon excitations.

As mentioned above, the primitive magnetic unit cell of MnWO_4 is composed of eight Mn spins in the collinear AF1 phase. Therefore, four twofold degenerate spin-wave branches

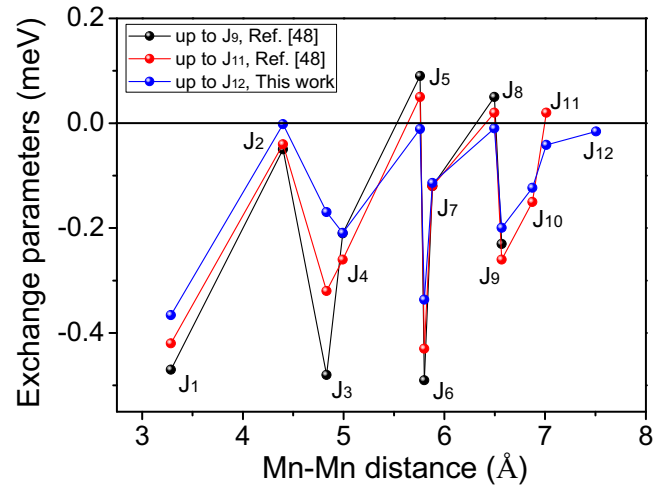


FIG. 3. Distance dependence of exchange interaction parameters. The parameters are obtained by considering Mn-Mn spin-exchange interaction up to the 9th, 11th, and 12th nearest neighbor, respectively.

are expected in zero field. However, the excitation spectrum at the zone center $\mathbf{Q} = (1/4, 1/2, 1/2)$ exhibits at least five resolvable excitations. This can be clearly seen in the individual energy scans plotted in Fig. 5(a). By considering different possibilities and evaluating the results of the refinements as a function of \mathbf{Q} , we found that it is impossible to describe the two low-lying energy excitations located in the zone center at $\omega_1 = 0.07(1)$ and $\omega_2 = 0.45(1)$ meV within the Heisenberg model. As demonstrated in Figs. 2(b) and 2(d), the dispersion as well as the intensities of the magnetic excitations can be well modeled as spin-wave excitations using the Hamiltonian in Eq. (2), if the low-lying excitations ω_1 and ω_2 are excluded. The fitting results exhibit excellent agreement with the experimental data for the spin-wave excitations and yield exchange parameters as $J_1 = -0.37(1)$, $J_2 = -0.002(1)$, $J_3 = -0.17(1)$, $J_4 = -0.21(1)$, $J_5 = -0.011(5)$, $J_6 = -0.34(1)$, $J_7 = -0.11(1)$, $J_8 = -0.010(5)$, $J_9 = -0.20(1)$, $J_{10} = -0.12(1)$, $J_{11} = -0.042(1)$, $J_{12} = -0.016(1)$ meV, and $D_S = 0.06(1)$, where all parameters are given in units of meV. All obtained exchange parameters are negative, which indicates that three-dimensional antiferromagnetic exchange interaction is the dominant interaction in MnWO_4 . It is also noticed that the strengths of some exchange interactions such as J_3 and J_6 , are comparable to that of the nearest-neighbor interaction J_1 , suggesting the existence of substantial magnetic frustration in MnWO_4 .

The spin-wave excitations in the AF1 phase of MnWO_4 have been studied previously by several groups, and the exchange parameters have been extracted from neutron-scattering experiments as well as from theory [46–48]. However, the parameters deduced in previous studies failed to reproduce the dispersion spectra in some aspects. In the latest reference [48], Ye *et al.* first modeled experimental results by considering nine exchange parameters at the beginning, but the authors found that more satisfied agreement can be achieved by considering exchange parameters up to J_{11} . As shown in Fig. 3, non-negligible values were obtained for J_{10}

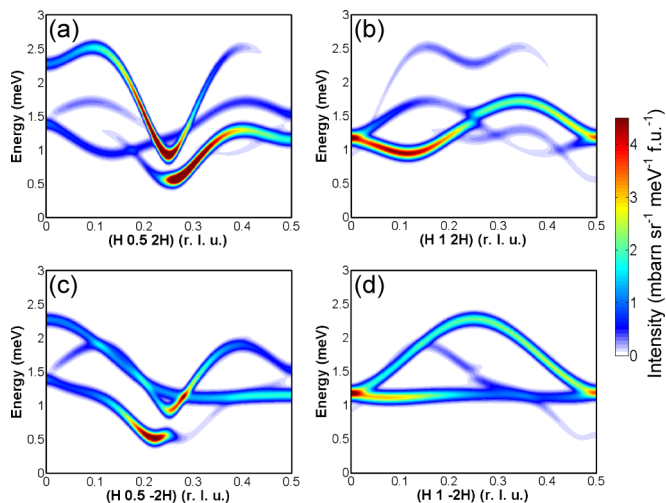


FIG. 4. (a) and (b) Calculated spin-wave excitation spectra of the AF1 phase along the $[1\ 0\ 2]$ direction with $K = 0.5$ and 1 , respectively. (c) and (d) Calculated spin-wave excitation spectra of the AF1 phase along the $[1\ 0\ -2]$ direction with $K = 0.5$ and 1 , respectively.

and J_{11} accompanied with the weakening or strengthening of other exchange interactions. However, it can be seen that the Heisenberg model including up to 11th exchange parameters is still not enough to fit the observed neutron spectra properly. For instance, the dispersion spectra along the $[1\ 0\ -2]$ direction through the magnetic peak $(1/4, 1/2, -1/2)$, especially the low-lying branch, cannot be reproduced properly, as indicated in Fig. 3 of Ref. [48]. In the present work, we found that the fitting of the spectra can be further improved if we include one more exchange parameter J_{12} . It is worth noting that the number of neighbors is two for exchange couplings J_1, J_2, \dots , and J_{11} , whereas it is four for exchange coupling J_{12} , indicating the considerable weight of exchange interaction between one given spin and its 12th nearest neighbor. The variation of exchange interaction parameters in the present work as a function of Mn-Mn distance is also plotted in Fig. 3 for comparison. It can be seen that most of the exchange parameters changed monotonically if more exchange parameters are taken into account. The obtained parameters can provide excellent agreement between theoretical and experimental results throughout the entire Brillouin zone. The calculated spin-wave excitation spectra along both $[1\ 0\ 2]$ and $[1\ 0\ -2]$ directions are plotted in Fig. 4. Compared with experimental and calculated neutron spectra shown in Ref. [48], the calculated spectra in the present work show significantly better agreement with the experimental data.

C. Electromagnon excitation and dispersion

Although the ME coupling in multiferroics will lead to the emergence of the electromagnon, the electromagnon excitation is not restricted to multiferroics since the macroscopic origin of dynamical ME coupling does not necessarily produce the multiferroic ground state. For instance, electromagnon excitations are observed in the paramagnetic phase of TbMnO_3 [49] and $\text{CuFe}_{1-x}\text{Ga}_x\text{O}_2$ [50] with collinear spin structure. In the AF1 phase of MnWO_4 , the Mn^{2+} spins are aligned collinearly

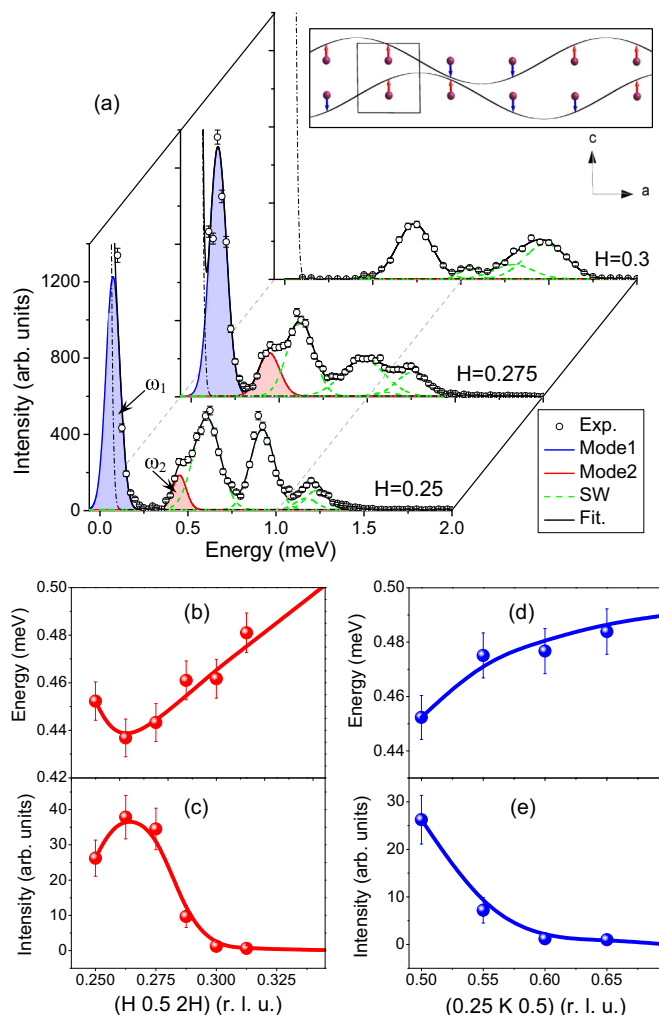


FIG. 5. (a) Representative magnetic excitation spectra around zone center $(1/4, 1/2, 1/2)$ at $1.5\ \text{K}$. The dashed lines are the estimated line shape for spin-wave excitations, while the spectral weights arising from electromagnon excitations are highlighted as the shaded areas under the curves. The dash-dotted line corresponds to the instrumental resolution. The inset illustrates the $\uparrow\uparrow\downarrow\downarrow$ spin configuration along the a axis, which can be treated as a special case of a modulated spin structure. (b) and (c) Dispersion relation and spectral weight of electromagnon excitation ω_2 along the $[1\ 0\ 2]$ direction. The solid lines are guides to the eye. (d) and (e) Dispersion relation and spectral weight of electromagnon excitation ω_2 along the $[0\ 1\ 0]$ direction.

along the easy axis with the spin direction alternating along the a axis as $\uparrow\uparrow\downarrow\downarrow$ [see the inset of Fig. 5(a)]. The $\uparrow\uparrow\downarrow\downarrow$ spin configuration can be considered as the special case of a modulated structure in the form of $\mathbf{S}_i = \mathbf{S}_0 \cdot \cos(2\pi k R_i + \pi/4)$ with $k = 1/4$. As for a spiral magnet, one phason mode and two rotation modes may contribute to the low-energy excitation. The observed two modes ω_1 and ω_2 in Fig. 5(a) can be attributed to the electromagnon excitations and they relate to the phason and rotation modes, respectively. In Figs. 5(b) and 5(c), the dispersion relation along the $[1\ 0\ 2]$ direction as well as the intensity change of electromagnon mode ω_2 extracted from the individual energy scans are plotted. Interestingly, an energy dip in the dispersion relation and a peak in the intensity

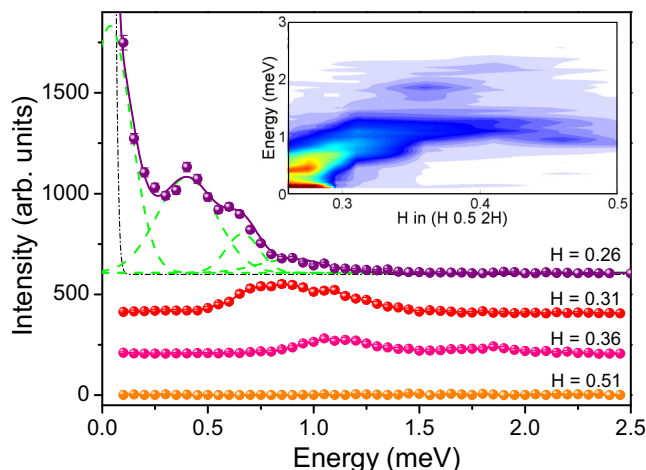


FIG. 6. (a) Selected energy scans at various wave vectors in the incommensurate AF2 phase at 10 K. The curves are shifted vertically for comparison. The inset shows the measured excitations in the AF2 phase around the zone center $\mathbf{Q} = (0.26, 0.5, 0.52)$ as a color plot.

are observed at $\mathbf{Q} = (0.26(1), 1/2, 0.52(2))$, which corresponds exactly to the magnetic propagation vector we find for the incommensurate AF2 phase [see Fig. 1(b)]. The minimal energy gap for the electromagnon ω_2 is associated with the magnetoelectric coupling effect in multiferroic MnWO_4 . In contrast to the dispersion along the $[1\ 0\ 2]$ direction, both energy and intensity of the electromagnon ω_2 along the $[0\ 1\ 0]$ direction evolve monotonically away from $\mathbf{Q} = (1/4\ 1/2\ 1/2)$, as shown in Figs. 5(d) and 5(e), indicating anisotropic dispersion behaviors of electromagnons in MnWO_4 .

Upon the increase in temperature, a transition from the collinear phase AF1 into the ferroelectric magnetic spiral phase AF2 occurs. In Fig. 6, representative scans of the low-energy excitations and their dispersion in the AF2 phase at 10 K are shown. Although the dispersion behavior persists in momentum space, the excitations broaden and soften in the AF2 phase in comparison to the AF1 phase. Nevertheless, four well-resolved excitation modes are identified by fitting the energy scans at the incommensurate wave vector $\mathbf{Q} = (0.26, 0.5, 0.52)$. Among these four modes, the broad mode located at $0.04(2)$ meV most likely corresponds to the ω_1 mode in the AF1 phase. As one of the electromagnon excitation modes, the ω_1 mode in the ferroelectric AF2 phase shows substantial spectrum weight gain about two times compared to the nonferroelectric AF1 phase. This underpins our identification of the low-energy excitation mode ω_1 as being associated with the dynamical magnetoelectric coupling.

Since electromagnon excitation is an electrically active spin excitation related to the multiferroic character in multiferroics, many efforts have been made aiming to elucidate the feature of the electromagnon in spin-driven multiferroics. The infrared spectroscopy and polarized neutron spectroscopy were accepted to be effective methods in evidencing the existence of the electromagnon [23,25]. In Ref. [51], the authors carried out optical spectroscopic investigations on MnWO_4 , but no signal from the electromagnon was found in the low-energy region of optical spectra with energy down to 0.62 meV, indicating that the electromagnon excitation in MnWO_4 might locate at

a lower-energy region. As a matter of fact, in the present work the observed two modes ω_1 and ω_2 are all below 0.6 meV. Nevertheless, it is impossible for us to identify the character of the low-lying energy modes from unpolarized neutron spectroscopy results. Further experimental work via polarized neutron spectroscopy is necessary in order to identify the observed magnon modes, thus to firmly confirm that the low-lying energy excitations are electromagnon excitations in nature.

IV. DISCUSSION

From our analysis of the spin-wave dispersion in the framework of the Heisenberg model, we deduced a spin-wave energy gap Δ of $0.61(1)$ meV and a single-ion anisotropy constant D_s of $0.06(1)$ meV for the AF1 phase. The observed anisotropy is considerable given the fact that in a purely ionic description manganese in MnWO_4 is an S -state Mn^{2+} ion with vanishing orbital moment. Full multiplet calculation shows that the magnetic anisotropy in MnWO_4 arises from the spin-orbit coupling and it is comparable in energy to the Dzyaloshinskii-Moriya interactions [52].

Compared to the spin-wave energy gap, the energy gaps of $0.07(1)$ and $0.45(1)$ meV for the two observed electromagnon excitations are relatively small, but of the same order of amplitude. If the inverse DM interaction is considered as the mechanism responsible for the multiferroic properties in MnWO_4 , the observed electromagnon excitations, which are associated with the magnetoelectric coupling, may arise from the DM exchange interaction instead of the Heisenberg interaction. Moreover, although the two observed electromagnon excitation modes cannot be described within the Heisenberg model, they do exhibit dispersive behavior characteristic for collective excitations. As shown in Fig. 5, the energy of ω_2 decreases slightly between $\mathbf{Q} = (1/4, 1/2, 1/2)$ and $(0.275, 1/2, 0.55)$, whereas the energy of ω_1 increases from $0.07(1)$ to $0.15(1)$ meV. The opposite dispersion behavior of the two electromagnon modes around the zone center suggests that the origins of the two excitation modes are different and/or these two excitation modes might couple with each other through hybridization effects. Further experimental works via complementary techniques and comprehensive dynamical structure calculations are required to get further insight into the nature of electromagnon excitations. It is also known that the application of magnetic field along the easy axis of MnWO_4 will lead to a switch of the polarization accompanied with the magnetic phase transition [53]. Therefore, it is interesting to investigate the evolution of electromagnon excitations upon the application of magnetic field in MnWO_4 . The behavior of electromagnon excitations across the field-induced transition between ferroelectric and paraelectric phases can be helpful to identify the character of electromagnon excitations [54,55], thus leading to a better understanding of the mechanism of magnetoelectric coupling in multiferroics with noncollinear spiral magnetic structure.

V. CONCLUSION

In summary, we present results of a comprehensive neutron-scattering study of the elementary magnetic excitations in multiferroic MnWO_4 . In addition to the well-known spin-wave

excitations, we demonstrate the existence of electromagnon excitations in both the paraelectric AF1 and the ferroelectric AF2 phases. The spin-wave excitations of MnWO_4 in the AF1 phase can be properly described by a Heisenberg model with local magnetic exchange coupling extending up to the 12th nearest neighbor. The analysis of spin-wave excitations suggests that the dominant interaction is antiferromagnetic in MnWO_4 . Competing antiferromagnetic exchange leads to frustration and gives rise to the modulated magnetic phases and the rich phase diagram. The spin-wave gap of 0.61(1) meV at 1.5 K amounts to roughly 1/4 of the zone boundary spin-wave energy. This relatively large value indicates the existence of rather strong spin-orbit interaction, despite the fact that Mn^{2+} is an S -state ion. The analysis of the low-energy excitation spectra implies the existence of collective electromagnon excitations, which reflect the strong ME coupling. Similar to the spin-wave excitations, the electromagnons also exhibit dispersive behavior with smaller but considerable energy

gaps at the zone center of 0.07(1) and 0.45(1) meV at 1.5 K, respectively. These modes persist in both the collinear magnetic and paraelectric AF1 phase below 7.8 K and the spin spiral ferroelectric AF2 phase between 7.8 and 12.6 K. Taking into account the assumed mechanism for multiferroicity in MnWO_4 based on the inverse DM effect, we argue that the electromagnons are associated with the magnetoelectric coupling arising from the Dzyaloshinskii-Moriya exchange mechanism, which is allowed in MnWO_4 due to the low symmetry and the rather strong spin-orbit coupling already evidenced by the spin-wave dispersion.

ACKNOWLEDGMENTS

The authors are grateful to J. Perþon for providing assistance with single-crystal growth and alignment. Y.X. acknowledges I.V. Solov'yev for helpful discussions.

-
- [1] T. Kimura, T. Goto, H. Shintani, K. Ishizaka, T. Arima, and Y. Tokura, *Nature (London)* **426**, 55 (2003).
- [2] N. Hur, S. Park, P. A. Sharma, J. S. Ahn, S. Guha, and S.-W. Cheong, *Nature (London)* **429**, 392 (2004).
- [3] M. Fiebig, *J. Phys. D* **38**, R123 (2005).
- [4] Y. Tokura and S. Seki, *Adv. Mater.* **22**, 1554 (2010).
- [5] S. Dong, J.-M. Liu, S.-W. Cheong, and Z. Ren, *Adv. Phys.* **64**, 519 (2015).
- [6] S.-W. Cheong and M. Mostovoy, *Nat. Mater.* **6**, 13 (2007).
- [7] Y. Tokura, S. Seki, and N. Nagaosa, *Rep. Prog. Phys.* **77**, 076501 (2014).
- [8] H. Katsura, N. Nagaosa, and A. V. Balatsky, *Phys. Rev. Lett.* **95**, 057205 (2005).
- [9] M. Mostovoy, *Phys. Rev. Lett.* **96**, 067601 (2006).
- [10] C. Jia, S. Onoda, N. Nagaosa, and J. H. Han, *Phys. Rev. B* **76**, 144424 (2007).
- [11] Y. J. Choi, H. T. Yi, S. Lee, Q. Huang, V. Kiryukhin, and S.-W. Cheong, *Phys. Rev. Lett.* **100**, 047601 (2008).
- [12] L. C. Chapon, P. G. Radaelli, G. R. Blake, S. Park, and S.-W. Cheong, *Phys. Rev. Lett.* **96**, 097601 (2006).
- [13] T. Goto, T. Kimura, G. Lawes, A. P. Ramirez, and Y. Tokura, *Phys. Rev. Lett.* **92**, 257201 (2004).
- [14] G. Lawes, A. B. Harris, T. Kimura, N. Rogado, R. J. Cava, A. Aharony, O. Entin-Wohlman, T. Yildirim, M. Kenzelmann, C. Broholm, and A. P. Ramirez, *Phys. Rev. Lett.* **95**, 087205 (2005).
- [15] Y. Yamasaki, S. Miyasaka, Y. Kaneko, J.-P. He, T. Arima, and Y. Tokura, *Phys. Rev. Lett.* **96**, 207204 (2006).
- [16] Y. Kitagawa, Y. Hiraoka, T. Honda, T. Ishikura, H. Nakamura, and T. Kimura, *Nat. Mater.* **9**, 797 (2010).
- [17] Y. Tokunaga, Y. Kaneko, D. Okuyama, S. Ishiwata, T. Arima, S. Wakimoto, K. Kakurai, Y. Taguchi, and Y. Tokura, *Phys. Rev. Lett.* **105**, 257201 (2010).
- [18] T. Kimura, J. C. Lashley, and A. P. Ramirez, *Phys. Rev. B* **73**, 220401 (2006).
- [19] Y. Tokunaga, N. Furukawa, H. Sakai, Y. Taguchi, T. Arima, and Y. Tokura, *Nat. Mater.* **8**, 558 (2009).
- [20] F. Kagawa, M. Mochizuki, Y. Onose, H. Murakawa, Y. Kaneko, N. Furukawa, and Y. Tokura, *Phys. Rev. Lett.* **102**, 057604 (2009).
- [21] S. Seki, H. Murakawa, Y. Onose, and Y. Tokura, *Phys. Rev. Lett.* **103**, 237601 (2009).
- [22] H. Katsura, A. V. Balatsky, and N. Nagaosa, *Phys. Rev. Lett.* **98**, 027203 (2007).
- [23] A. Pimenov, A. A. Mukhin, V. Yu. Ivanov, V. D. Travkin, A. M. Balbashov, and A. Loidl, *Nat. Phys.* **2**, 97 (2006).
- [24] Y. Takahashi, R. Shimano, Y. Kaneko, H. Murakawa, and Y. Tokura, *Nat. Phys.* **8**, 121 (2012).
- [25] D. Senff, P. Link, K. Hradil, A. Hiess, L. P. Regnault, Y. Sidis, N. Aliouane, D. N. Argyriou, and M. Braden, *Phys. Rev. Lett.* **98**, 137206 (2007).
- [26] S. P. P. Jones, S. M. Gaw, K. I. Doig, D. Prabhakaran, E. M. Hetroy Wheeler, A. T. Boothroyd, and J. Lloyd-Hughes, *Nat. Commun.* **5**, 3787 (2014).
- [27] T. Finger, K. Binder, Y. Sidis, A. Maljuk, D. N. Argyriou, and M. Braden, *Phys. Rev. B* **90**, 224418 (2014).
- [28] O. Heyer, N. Hollmann, I. Klassen, S. Jodlauk, L. Bohaty, P. Becker, J. A. Mydosh, T. Lorenz, and D. Khomskii, *J. Phys.: Condens. Matter* **18**, L471 (2006).
- [29] K. Taniguchi, N. Abe, T. Takenobu, Y. Iwasa, and T. Arima, *Phys. Rev. Lett.* **97**, 097203 (2006).
- [30] A. H. Arkenbout, T. T. M. Palstra, T. Siegrist, and T. Kimura, *Phys. Rev. B* **74**, 184431 (2006).
- [31] R. P. Chaudhury, B. Lorenz, Y. Q. Wang, Y. Y. Sun, and C. W. Chu, *Phys. Rev. B* **77**, 104406 (2008).
- [32] F. Ye, Y. Ren, J. A. Fernandez-Baca, H. A. Mook, J. W. Lynn, R. P. Chaudhury, Y.-Q. Wang, B. Lorenz, and C. W. Chu, *Phys. Rev. B* **78**, 193101 (2008).
- [33] R. P. Chaudhury, F. Ye, J. A. Fernandez-Baca, B. Lorenz, Y. Q. Wang, Y. Y. Sun, H. A. Mook, and C. W. Chu, *Phys. Rev. B* **83**, 014401 (2011).
- [34] F. Ye, S. Chi, J. A. Fernandez-Baca, H. Cao, K.-C. Liang, Y. Wang, B. Lorenz, and C. W. Chu, *Phys. Rev. B* **86**, 094429 (2012).
- [35] H. Sagayama, K. Taniguchi, N. Abe, T. H. Arima, M. Soda, M. Matsuura, and K. Hirota, *Phys. Rev. B* **77**, 220407(R) (2008).
- [36] T. Finger, D. Senff, K. Schmalzl, W. Schmidt, L. P. Regnault, P. Becker, L. Bohatý and M. Braden, *Phys. Rev. B* **81**, 054430 (2010).

- [37] D. Niermann, C. P. Grams, P. Becker, L. Bohatý, H. Schenck, and J. Hemberger, *Phys. Rev. Lett.* **114**, 037204 (2015).
- [38] C. M. N. Kumar, Y. Xiao, P. Lunkenheimer, A. Loidl, and M. Ohl, *Phys. Rev. B* **91**, 235149 (2015).
- [39] P. Toledano, B. Mettout, W. Schranz, and G. Krexner, *J. Phys.: Condens. Matter* **22**, 065901 (2010).
- [40] I. V. Solovyev, *Phys. Rev. B* **87**, 144403 (2013).
- [41] A. Schneidewind and P. Čermák, *J. Large-Scale Res. Faci.* **1**, A12 (2015).
- [42] G. Lautenschläger, H. Weitzel, T. Vogt, R. Hock, A. Böhm, M. Bonnet, and H. Fuess, *Phys. Rev. B* **48**, 6087 (1993).
- [43] A. W. Sleight, *Acta Crystallogr. B: Struct. Crystallogr. Cryst. Chem.* **28**, 2899 (1972).
- [44] T. Brückel and W. Prandl, *Z. Phys. B: Condens. Matter* **73**, 57 (1988).
- [45] S. W. Lovesey, *Theory of Neutron Scattering from Condensed Matter* (Oxford University Press, Oxford, 1984).
- [46] H. Ehrenberg, H. Weitzel, H. Fuess, and B. Hennion, *J. Phys.: Condens. Matter* **11**, 2649 (1999).
- [47] C. Tian, C. Lee, H. Xiang, Y. Zhang, C. Payen, S. Jobic, and M. H. Whangbo, *Phys. Rev. B* **80**, 104426 (2009).
- [48] F. Ye, R. S. Fishman, J. A. Fernandez-Baca, A. A. Podlesnyak, G. Ehlers, H. A. Mook, Y. Wang, B. Lorenz, and C. W. Chu, *Phys. Rev. B* **83**, 140401(R) (2011).
- [49] D. Senff, N. Aliouane, D. N. Argyriou, A. Hiess, L. P. Regnault, P. Link, K. Hradil, Y. Sidis, and M. Braden, *J. Phys.: Condens. Matter* **20**, 434212 (2008).
- [50] S. Seki, N. Kida, S. Kumakura, R. Shimano, and Y. Tokura, *Phys. Rev. Lett.* **105**, 097207 (2010).
- [51] W. S. Choi, K. Taniguchi, S. J. Moon, S. S. A. Seo, T. Arima, H. Hoang, I.-S. Yang, T. W. Noh, and Y. S. Lee, *Phys. Rev. B* **81**, 205111 (2010).
- [52] N. Hollmann, Z. Hu, T. Willers, L. Bohaty, P. Becker, A. Tanaka, H. H. Hsieh, H.-J. Lin, C. T. Chen, and L. H. Tjeng, *Phys. Rev. B* **82**, 184429 (2010).
- [53] K. Taniguchi, N. Abe, H. Sagayama, S. Ohtani, T. Takenobu, Y. Iwasa, and T. Arima, *Phys. Rev. B* **77**, 064408 (2008).
- [54] A. Pimenov, A. Shuvaev, A. Loidl, F. Schrettle, A. A. Mukhin, V. D. Travkin, V. Yu. Ivanov, and A. M. Balbashov, *Phys. Rev. Lett.* **102**, 107203 (2009).
- [55] S. Holbein, P. Steffens, T. Finger, A. C. Komarek, Y. Sidis, P. Link, and M. Braden, *Phys. Rev. B* **91**, 014432 (2015).